Diffusive and ballistic current spin polarization in magnetron-sputtered $L1_0$-ordered epitaxial FePt

Klaus M. Seemann,[1,*] Vincent Baltz,[1] Maureen MacKenzie,[2] John N. Chapman,[2] Bryan J. Hickey,[1] and Christopher H. Marrows[1,†]

[1]*School of Physics and Astronomy, University of Leeds, Leeds LS2 9JT, United Kingdom*

[2]*Department of Physics and Astronomy, University of Glasgow, Glasgow G12 8QQ, United Kingdom*

(Received 11 July 2007; revised manuscript received 21 September 2007; published 26 November 2007)

We report on the structural, magnetic, and electron transport properties of an $L1_0$-ordered epitaxial iron-platinum alloy layer fabricated by magnetron sputtering on a MgO (001) substrate. The film studied displayed a long-range chemical order parameter of $S \sim 0.90$, and hence has a very strong perpendicular magnetic anisotropy. In the diffusive electron transport regime, for temperatures ranging from 2 to 258 K, we found hysteresis in the magnetoresistance mainly due to electron scattering from magnetic domain walls. At 2 K, we observed an overall domain wall magnetoresistance of about 0.5%. By evaluating the spin current asymmetry $\alpha = \sigma_\uparrow / \sigma_\downarrow$, we were able to estimate the diffusive spin current polarization. At all temperatures ranging from 2 to 258 K, we found a diffusive spin current polarization of greater than 80%. To study the ballistic transport regime, we have performed point-contact Andreev-reflection measurements at 4.2 K. We obtained a value for the ballistic current spin polarization of ~42% (which compares very well with that of a polycrystalline thin film of elemental Fe). We attribute the discrepancy to a difference in the characteristic scattering times for oppositely spin-polarized electrons, such scattering times influencing the diffusive but not the ballistic current spin polarization.

DOI: 10.1103/PhysRevB.76.174435 PACS number(s): 72.25.Ba, 73.43.Qt, 75.50.Bb

I. INTRODUCTION

Recent advances in the research field of current-induced magnetization switching and current-driven magnetization dynamics,[1] as well as the developments in the hard disk drive industry to change the magnetic storage process to perpendicular magnetic recording, cause a resurgence of interest in ultrathin film magnetic materials with out-of-plane magnetic anisotropy. One way to achieve this is to exploit magnetocrystalline anisotropy in an epitaxial film.[2–4] This upsurge in research interest in epitaxial material exhibiting a high perpendicular uniaxial anisotropy constant $K_\perp$ has been stimulated especially since sputter deposition now yields epitaxial thin films of an ordering quality comparable to molecular beam epitaxy (MBE).[5–8] The very high values of $K_\perp$ now available lead to domain walls of a very narrow thickness δ_W, and this makes fundamental physical phenomena like magnetoresistance (MR) due to electron scattering at magnetic domain walls an easily measurable effect.[9–11] After some early experimental work,[12–14] domain wall scattering is undergoing something of a renaissance as materials preparation and nanofabrication technologies improve.[15–18]

This effect of an increased electric resistivity in the presence of magnetic domain walls in a ferromagnetic thin film was measured by Viret *et al.* for films of Ni and Co.[19] This group developed a semiclassical model based on spin mistracking as the electrons cross the wall, which they used to interpret their data. (This type of model was necessary since quantum mechanical reflection of electrons from a domain wall potential step will be extremely small unless the wall is of extreme abruptness.[20,21]) A more rigorous quantum mechanical model, based on a Hamiltonian employed to calculate giant magnetoresistance in a spin-split system, was used by Levy and Zhang to treat the same physics.[22] It is possible to use this model to determine the polarization of a diffusive current by measuring domain wall resistance.[11]

This paper concentrates on the electron transport properties of the epitaxial $L1_0$-ordered iron alloy FePt in both the diffusive and the ballistic regimes. In particular, we have measured the spin polarization of the current in two different transport regimes: diffusive and ballistic. The strong uniaxial anisotropy, arising from the high degree of long-range chemical order in our ordered alloy epilayers, leads to a dense stripe domain structure with narrow walls. These give rise to an easily measurable magnetoresistance associated with the extra resistance as the electrons pass through these walls. By using the Levy-Zhang model,[22] this can be used to infer the spin polarization of these diffusive current-carrying electrons, which we find to exceed 80% at all temperatures from 2 to 258 K. We also determined the ballistic current spin polarization by the widely used point-contact Andreev-reflection (PCAR) method.[23,24] We found a spin polarization of ~42%, close to that reported for elemental 3*d* ferromagnets.

II. SAMPLE PREPARATION AND CHARACTERIZATION

The samples were prepared by conventional dc magnetron sputter deposition on polished MgO (001) substrates. We used a 4%-hydrogen-in-argon sputter gas mixture to prevent any film oxidation during growth at high temperatures. The FePt magnetic thin film was sputtered by codeposition directly onto the substrates at a substrate temperature of 1000 K and at a deposition rate of 0.1–0.2 $Å/s^{-1}$. Here we will describe the properties of a 31-nm-thick film, which has one of the highest degrees of chemical order we have achieved, having grown several dozen such samples to optimize our deposition process.

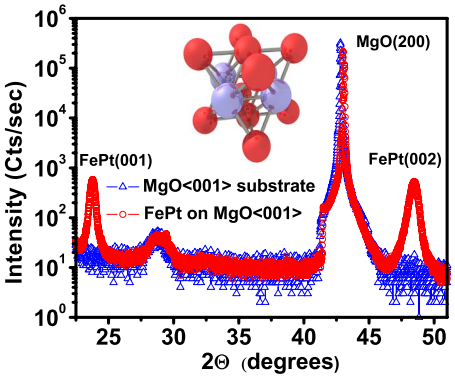

FIG. 1. (Color online) Θ-2Θ x-ray crystallography scan for $L1_0$-ordered FePt of a film thickness of 31 nm (circles) The MgO (001) substrate scan is included for comparison (triangles). The inset illustrates a unit cell of the face-centered tetragonal lattice of FePt. The Fe atoms (top and bottom planes) and Pt atoms (middle plane) form alternating *a*-*b* planes. The *c* axis lies normal to these planes and forms the magnetic easy axis. This is the growth direction in our epitaxial film.

For structural characterization of the epitaxial $L1_0$-ordered FePt thin films, we carried out Θ-2Θ x-ray diffraction scans using Cu $K\alpha$ radiation in order to determine the long-range order parameter S $(0 \leqslant S \leqslant 1)$ according to

$$S = r_\alpha + r_\beta - 1 = \frac{(r_\alpha - x_A)}{y_\beta} = \frac{(r_\beta - x_B)}{y_\alpha}. \quad (1)$$

Here x_a and x_b are the atom fractions of the two components, y_α and y_β are the fractions of the lattice site types α and β in the ordered structure, and r_α and r_β are the fractions of each type of lattice site occupied by the correct type of atom, A on α and B on β.[25–27] A typical Θ-2Θ scan of an $L1_0$-ordered FePt is displayed in Fig. 1. The presence of the (001) peak is normally forbidden by the structure factor for face-centered crystal lattices, and so its observation here confirms that there is preferential ordering on the alternating α and β planes. The (001) peak and (002) peaks were fitted with Lorentzian line shapes to yield the integrated intensities. Following the standard procedure, described in, e.g., Ref. 25, these integrated intensities, together with the peak positions, Lorentz polarization factors, and atomic scattering factors, can be used to give a value for S. We found $S=0.90\pm0.05$ for the particular film of thickness of 31.0 nm that we discuss in detail in this paper, and routinely obtain $S>0.80$ in our sputtered films. We calculated the film thickness via Kiessig fringes obtained in low-angle x-ray reflectometry measurements.

We performed transmission electron microscopy on an FEI Tecnai F20 to provide structural information on our material.[28] The cross-sectional high-resolution transmission electron microscopy (HRTEM) image in Fig. 2 from a comparable sample, taken with the electron beam aligned parallel to the [100] or [010] zone axis of the MgO substrate confirms the high quality of our epitaxial FePt layers on the MgO(001) substrates. The $L1_0$ ordering of the FePt was verified by selected area electron diffraction (see Fig. 3), which

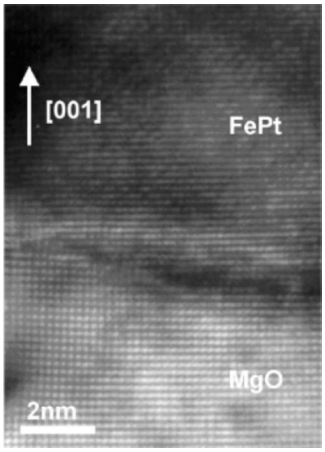

FIG. 2. Lattice structure as obtained from HRTEM of the $L1_0$-ordered FePt thin film grown on MgO(001). The [001] direction is the growth direction in our epitaxial film.

shows the diffraction pattern from a cross-sectional TEM of the same sample of FePt on MgO(001). The high degree of alignment between the MgO and FePt structures is clearly depicted. The {002} and {022} reflections from the face-centered cubic MgO substrate are marked with red crosses and show the expected fourfold symmetry associated with the [100] zone axis. The remaining reflections are from the FePt layer and index as the [100] zone axis of $L1_0$-ordered face-centered tetragonal FePt. The presence of the (001) superlattice spots confirms the $L1_0$ ordering of FePt. Using a lattice parameter of 4.21 Å for MgO as a calibration, we obtain $a=3.85$ Å and $c=3.76$ Å for the FePt structure. This gives a lattice mismatch of 8.5% between the MgO substrate and FePt layer. Hence, we would expect a misfit dislocation at the interface roughly every 11 atomic spacings, and a careful examination of a Fourier filtered image (not shown) reveals these. We also observe a much smaller number of dis-

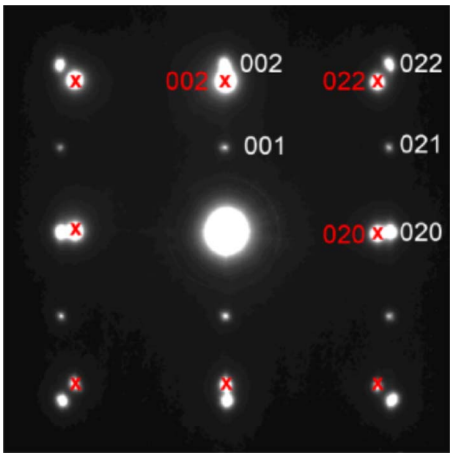

FIG. 3. (Color online) Selected area electron diffraction pattern from a cross-sectional TEM sample of FePt on MgO(001). The (001) superlattice spots confirm the $L1_0$-ordered FePt structure of the FePt thin film. The diffracted spots associated with the MgO(001) substrate are marked with crosses.

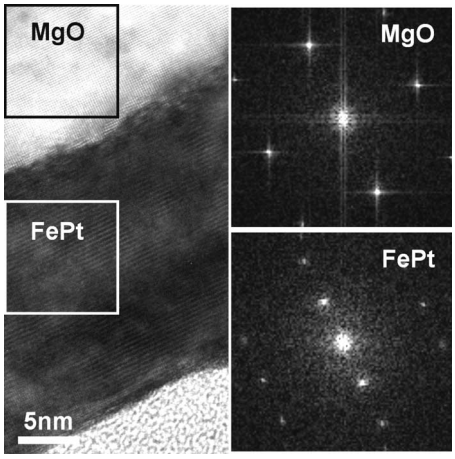

FIG. 4. HRTEM image of an $L1_0$-ordered FePt thin film grown on MgO(001). Inset are FFT patterns obtained from the regions of the single-crystal MgO substrate and the epitaxial FePt layer marked with boxes. It can be seen that the superlattice spots are associated with the FePt layer.

locations in the bulk of the film, at roughly the same density as in the MgO substrate. These filtered HRTEM images also reveal that the $L1_0$ FePt film relaxes the strain arising from the lattice mismatch within the first ten FePt atomic bilayers. In Fig. 4 we show another image with a larger field of view. Fast Fourier transform (FFT) patterns obtained from the boxed areas in Fig. 4, and shown as insets, confirm that the superlattice spots seen in the electron diffraction pattern are associated with the $L1_0$ order in the FePt layer.

A quantitative analysis of the strong out-of-plane magnetic anisotropy of the $L1_0$-ordered FePt film was carried out by vibrating-sample magnetometry in the out-of-plane geometry as well as the in-plane geometry, with representative hysteresis loops shown in Fig. 5(a). The uniaxial magnetocrystalline anisotropy constant $K_\perp$ was calculated from[29]

$$K_\perp = \mu_0 \int_0^{M_{\text{sat}}} (H_{\text{hard axis}} - H_{\text{easy axis}}) dM + K_{\text{demag}}, \quad (2)$$

where the extra term $K_{\text{demag}} = \frac{1}{2}\mu_0 M_{\text{sat}}^2$ accounts for the demagnetization field within the sample. $H_{\text{hard axis}}$ and $H_{\text{easy axis}}$ are the magnetic fields applied in and normal to the film plane, respectively. For $T = 276$ K, we found $K_\perp = 1.9 \pm 0.2$ MJ m^{-3}, $M_{\text{sat}} = 1.0 \pm 0.1$ MA m^{-1}, and $A = 14.2 \pm 4$ pJ m^{-1}. We deduced the zero-kelvin exchange stiffness A from a $T^{3/2}$ Bloch law fit of the temperature dependence of the saturation magnetization[29] and assumed that $A(T)$ follows a mean-field behavior proportional to $M_{\text{sat}}(T)$: the data and fitted curve are shown in Fig. 5(b). The temperature dependence of $K_\perp$ is shown in Fig. 5(c). Experimental micromagnetic data were not available for $T < 50$ K due to the large signal that arises at low temperatures caused by paramagnetic impurities in the substrate (typically at the parts per million level in epiready MgO). The values we obtain compare reasonably well with the micromagnetic parameters recently reported for $L1_0$-ordered FePt thin films grown by

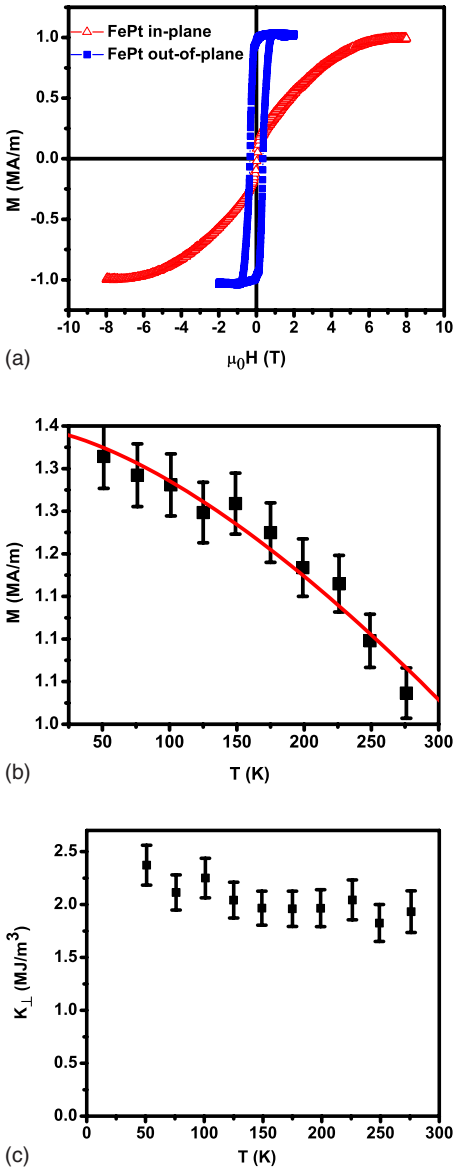

FIG. 5. (Color online) (a) Hysteresis loops for the 31-nm-thick $L1_0$-ordered FePt film obtained by vibrating-sample magnetometry in the in-plane and out-of-plane geometry at $T = 276$ K, (b) the saturation magnetization together with a Bloch law fit, and (c) the uniaxial anisotropy constant $K_\perp$ as a function of temperature.

molecular beam epitaxy and magnetron sputtering of other groups.[7,8,30–33]

We imaged the magnetic domain structure of FePt by magnetic force microscopy (MFM) at room temperature in zero field, as shown in Fig. 6(a). The sample was demagnetized using an alternating magnetic field of decreasing amplitude. The cantilevers had a resonant frequency of 65 kHz and a spring constant of 1–5 N/m. The CoCr-coated Si tip was vertically magnetized prior to imaging. For optimal contrast we kept the tip-surface distance constant at a value in the range 20–25 nm. The average magnetic domain width of the demagnetized state was obtained by a power-spectrum analysis and resulted in a domain width of $D = 170 \pm 15$ nm for the 31.0-nm-thick sample. The domain structure exhibits

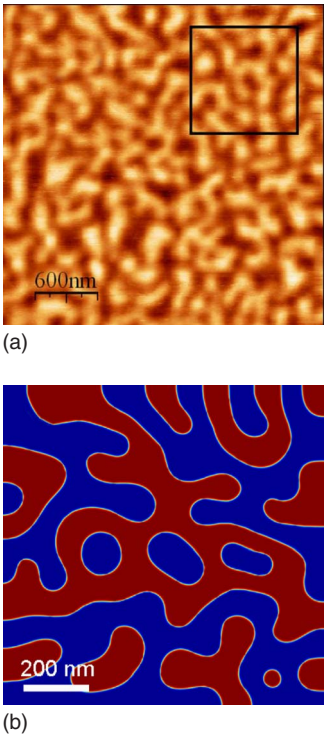

FIG. 6. (Color online) Magnetic force image (a) showing the typical labyrinth domain structure of the demagnetized $L1_0$-ordered FePt film in zero magnetic field. The bright and dark areas mark magnetic domains of opposite perpendicular magnetization. A power spectrum analysis of such images leads to an average domain width of $\sim 170 \pm 20$ nm. Micromagnetic simulation (b) of the domain structure of a 1×1 μm^2 FePt thin film of 30 nm thickness using the OOMMF code and experimentally determined micromagnetic parameters. The red and blue (bright and dark) regions mark areas of opposite perpendicular magnetization. The typical domain width can be seen to be $D \sim 150$ nm. The black square in (a) shows a region of the same size as that simulated and shown in (b).

the typical interconnected dense stripe domain structure known from $L1_0$-ordered binary iron alloys.[7,34,35]

We carried out micromagnetic simulations of this domain structure in the sample using the oommf code,[36] the results of which are shown in Fig. 6(b). The cell size used was 1×1 nm^2 within the film plane and 15 nm perpendicular to the film plane, and a six-nearest-neighbor exchange interaction for the magnetic energy terms of adjacent cells was employed. Although thermal activation effects are not taken into account in this type of micromagnetic code, we were nevertheless able to simulate the domain structures in our material at finite temperatures using the appropriate values of the micromagnetic parameters $A(T)$, $K(T)$, and $M(T)$ as determined from vibrating-sample magnetometry, as we are not concerned with thermal activation effects when determining the equilibrium domain structure. Our simulation yields an average domain width $D \sim 150$ nm at room temperature for a 30 nm thick film obtained from a Fourier analysis of the oommf output. The analytical result obtained from the Kaplan-Gehring model[37] is ~ 130 nm at room temperature and ~ 90 nm at 50 K, so the temperature dependence of the domain strip width is quite weak.

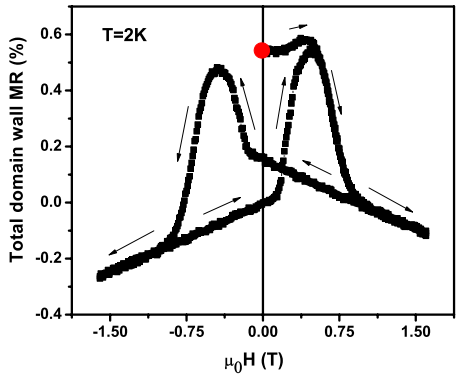

FIG. 7. (Color online) Magnetoresistance vs applied field of $L1_0$-ordered FePt obtained by a dc in-line four-terminal measurement at $T=2$ K in the perpendicular field geometry. The dot marks the resistance in the demagnetized state of the sample, at the start of the virgin branch of the hysteresis loop.

We also estimated the average width of an individual domain wall analytically from

$$\delta_W \simeq \pi \sqrt{\left(\frac{A}{K_\perp}\right)}. \tag{3}$$

Using our experimentally determined micromagnetic parameters, we obtain $\delta_W \sim 8-9$ nm at all temperatures in good agreement with our micromagnetic simulations. Such narrow wall thicknesses are extremely difficult to measure experimentally. Such narrow Bloch-type domain walls may be found in many hard magnet materials such as NdFeB or SmCo. Their effect on thin film electron transport properties such as domain wall resistance is particularly interesting. Narrower walls are available only in a very few magnetic materials [e.g., at low temperatures in $SrRuO_3$ (Ref. 38)].

III. ELECTRON TRANSPORT PROPERTIES

A. Transport in the diffusive regime

We first describe the diffusive transport properties of $L1_0$-ordered FePt. We performed magnetotransport measurements at temperatures ranging from 2 to 258 K using an in-line four-terminal setup with the magnetic field applied normal to the film plane. We found a hysteretic part of the magnetoresistance of $(\Delta\rho/\rho)_{\text{domain}}=0.55\%$ at 2 K and $(\Delta\rho/\rho)_{\text{domain}}=0.26\%$ at 258 K, associated with the creation and annihilation of domain walls as the film switches its magnetization direction. A typical MR hysteresis loop is shown in Fig. 7. From previous studies on $L1_0$-ordered FePd thin films,[11] we know that a sufficiently high quality factor $Q=2K_\perp/\mu_0 M^2$ similar to the one in this case, $Q \approx 2.2$, is a good indication that the anisotropy magnetoresistance contribution of Néel closure caps on the domain walls cannot account for this effect and is small enough to be neglected. The asymmetry of the MR loops arises through the extraordinary Hall effect, caused by large spin-orbit interaction in FePt, and the minute misalignment of our voltage probes. This effect can be easily subtracted to give the true domain wall

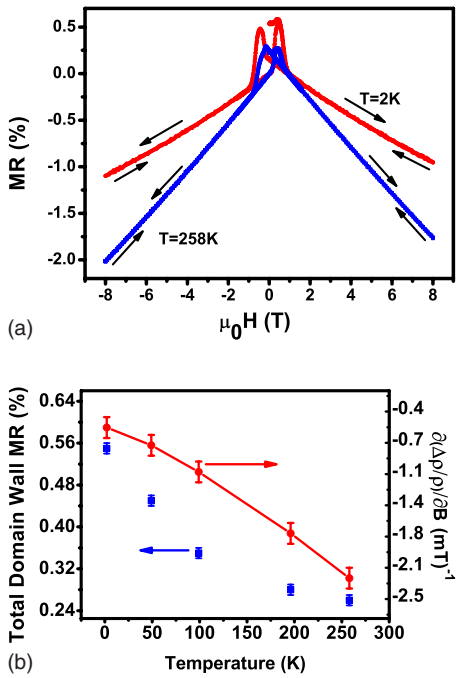

FIG. 8. (Color online) (a) Hysteretic MR loops obtained for $L1_0$-ordered FePt at $T=2$ and 258 K in the perpendicular geometry. A strong linear high-field magnetoresistance is evident in both cases. (b) Total domain wall MR (squares) and high-field MR slope (circles) vs temperature for an $L1_0$-ordered FePt thin film of a thickness of 31 nm. The solid line is a fit to the data as described in the text.

MR. We will discuss the extraordinary Hall effect in films such as these in more detail elsewhere.

We find the domain wall MR to be approximately twice as large as compared to those reported on $L1_0$-ordered FePt films grown by molecular beam epitaxy,[10] even though our film had a rather high electrical resistivity of $\rho=35\ \mu\Omega$ cm (at 2 K), which implies that the mean free path is in the nanometer regime. The residual resistivity ratio is $R_{258\ \mathrm{K}}/R_{2\ \mathrm{K}}=2.4$. The temperature dependence of the domain wall MR is shown in Fig. 8(a) and exhibits an almost linear behavior with temperature.

In addition to the hysteretic part of the MR, we observe a reversible linear part at high fields. We have extracted the high-field MR slopes $\partial(\Delta\rho/\rho)/\partial B$ at an applied magnetic field of 5 T at various temperatures [Fig. 8(b)]. In Fe, Co, and Ni, such a negative and linear MR was found by Raquet *et al.*[39] to be caused by the influence of a magnetic field on the spin mixing resistivity. There, the main role is played by spin-flip *s-d* interband and intraband scattering due to electron-magnon scattering. The data in Fig. 8(b) can be fitted with the expression given by Raquet *et al.*[40] quite well, with the exception that a substantial linear MR $[\partial(\Delta\rho/\rho)/\partial B=-0.0054\ \mathrm{T}^{-1}]$ remains even at the lowest temperatures in this film, which must be added as an additional constant term. (We observe a negligibly small contribution proportional to B^2 as was the case in FePd.[11]) Subsequently, we could fit the temperature dependence of the high-field MR slope [Fig. 8(b)] according to Raquet *et al.*[40] This procedure yields a magnon mass renormalization constant of $d_1\approx-6.0\times10^{-7}$, which is comparable with that of pure 3*d* metals,[41] and less negative than that found previously in MBE-grown FePd.[11] We do not have a simple explanation for the temperature-independent part of the high-field linear MR, although we note that magnetoresistances in thin films can take on a variety of unexpected forms.[42]

Furthermore, we have used our magnetoresistance data to compute the spin-current asymmetry parameter α in $L1_0$-ordered FePt based on the Levy-Zhang spin-mistracking model.[22] The spin asymmetry of the current depends on the spin-resolved conductivities $\sigma_\uparrow,\sigma_\downarrow$ (or spin-resolved resistivities $\rho_\uparrow,\rho_\downarrow$) of the majority and minority spin channels and is given by $\alpha=\sigma_\uparrow/\sigma_\downarrow=\rho_\downarrow/\rho_\uparrow$.

The Levy-Zhang model describes the MR only in the wall region, whereas we have measured our entire film. We estimated the volume fraction of walls by measuring the total wall length λ_W in the MFM image of scan width Λ and multiplying this by the wall thickness δ_W to obtain the total area occupied by walls, out of a total area of Λ^2. This procedure yields a volume fraction accounting for the fact that we do not have a parallel stripe domain state, but rather a labyrinth structure, and yields a value approximately 1.3 times greater than the ideal stripe domain value δ_W/D. Thus one obtains for an isotropic labyrinth domain state a domain wall magnetoresistance of[11]

$$\frac{\Delta\rho}{\rho}=\frac{1}{5}\left(\frac{\lambda_W\delta_W}{\Lambda^2}\right)\left(\frac{\pi\hbar^2k_F}{4mJ\delta_W}\right)^2\frac{(\alpha-1)^2}{2\alpha}\left(4+\frac{10\sqrt{\alpha}}{\alpha+1}\right), \quad (4)$$

where k_F is the Fermi wave vector, m is the effective electron mass, and J is the Stoner exchange-splitting energy. It is to be noted that this formula yields the same $\Delta\rho/\rho$ for both α and $1/\alpha$, equivalent to saying that we are insensitive to the sign of the polarization. Based on the assumption that the majority carriers are *s*-like, we take m to be equal to the free electron mass, assume the value of k_F to be 2 Å^{-1} (a typical value for a metal), and take a value for the Stoner exchange splitting to be $J(0)=2.0$ eV based on the splitting of the density of states seen in the results of band structure calculations.[43] We appropriately scaled the domain wall volume fraction based on the analytical values for δ_W and D for different temperatures. Figure 9(a) shows the spin current asymmetry α of $L1_0$-ordered FePt calculated according to Eq. (4). A strong temperature dependence of α is clearly visible, with a decay of the spin current asymmetry from $\alpha=16$ to 10 in the temperature range between 2 and 258 K. It is then straightforward to obtain the diffusive current spin polarization of $L1_0$-ordered FePt from

$$P_{\mathrm{diffusive}}=\left(\frac{\sigma_\uparrow-\sigma_\downarrow}{\sigma_\uparrow+\sigma_\downarrow}\right)=\left(\frac{\alpha-1}{\alpha+1}\right), \quad (5)$$

which is shown in Fig. 9(b). For a temperature of 258 K, we found a diffusive spin current polarization of $P_{\mathrm{diffusive}}=0.82\pm0.04$, whereas $P_{\mathrm{diffusive}}=0.88\pm0.02$ at $T=4.2$ K. The uncertainties in these polarization values are determined from the uncertainties in the α values, which in turn were computed using Eq. (4), and also taking into account the uncertainties of the micromagnetic parameters $K_\perp$, M and A

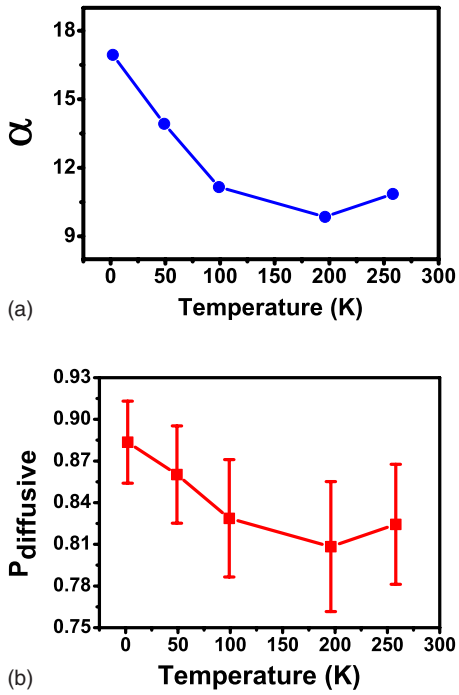

FIG. 9. (Color online) T dependence of the spin resistivity asymmetry α (a) and the diffusive current spin polarization $P_{\text{diffusive}}$ (b).

taken to evaluate the domain wall dilution. The final uncertainties are small since the diffusive polarization is rather insensitive to the value of α when $\alpha \gg 1$.

B. Transport in the ballistic regime

We performed point-contact Andreev-reflection measurements in order to directly probe for the ballistic current spin polarization of $L1_0$-ordered FePt.[16,23,24,44–47] The concept of this method is based on the fact that, for applied bias voltages within the gap of the superconductor, it is physically impossible to inject or extract single electrons, but only Cooper pairs. As the Andreev-reflection process[48] is the coherent back reflection of a charge carrier hole into the ferromagnetic sample following the capturing of an opposite-spin electron to form a Cooper pair inside the superconducting tip, one essentially probes for the number of unpaired electrons, straightforwardly giving the ballistic spin current polarization of the ferromagnet.

The point contact was controlled mechanically at 4.2 K, in a liquid helium bath, between a superconducting niobium tip and the FePt thin film. We used the same sample as for the diffusive transport characterization. A bias voltage was applied across the point contact and the differential conductance was recorded via a four-probe technique. ac lock-in detection with a 0.1 mV amplitude and a 5 kHz frequency was used. The tips were repeatedly brought into contact with the sample and the dependency of the differential conductance on the sample-tip bias voltage were recorded for various contact resistances. A typical curve is shown in Fig. 10. As also displayed in Fig. 10, the data were corrected for the

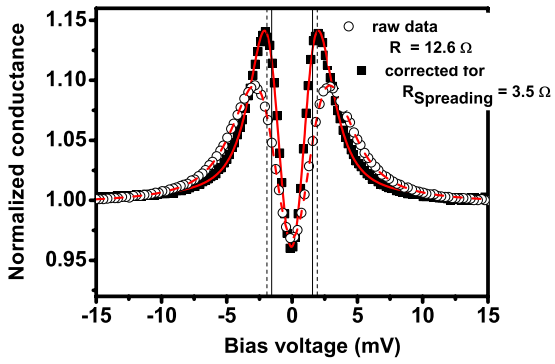

FIG. 10. (Color online) Normalized conductance vs bias voltage as obtained by PCAR at $T=4.2$ K before (circles) and after (squares) correction from the spreading resistance as defined in the text, together with the corresponding fits according to the modified BTK model (dashed and continuous lines). The fitting parameters are discussed in the text and given in the following figure. The vertical lines indicate the values of the deduced gaps before (dashed line) and after (continuous line) correction.

contribution of spreading resistances within the film, as deduced from our measurements. Spreading resistances are commonly found when the resistances of the point contact (of around 10 Ω in our case) are of the same order of magnitude as the resistance of the film (here around 80 Ω), and a common telltale sign is that the superconducting gap is significantly overestimated. It is then necessary to correct both voltage bias and differential conductance data for this additional series resistance.[49] However, the effect of correction on polarisation is not large in our case, since the ratio of subgap to quasiparticle conductance never strays too far from unity at any value of bias, because the polarization is close to 50%.

From the typical resistances of the point contacts ranging between 4 and 15 Ω, and using the Sharvin formula, we calculate an effective point-contact characteristic size of around 5–15 nm.[49,50] Such a value is much smaller than the characteristic micrometer size of the terminated apex of our tip, as measured by scanning electron microscopy. Indeed, as is usually the case, our contact results in multiple effective nanometric point contacts,[50] where electron transport across the ferromagnet-superconductor interface is ballistic.

The conductance vs bias voltage data were fitted in the standard way, employing a modified Blonder-Tinkham-Klapwijk (BTK) model,[51] which describes the crossover from metallic to tunnel junction behavior of a microconstriction contact between a semiconductor and a superconductor based on the Bogoliubov equations. Four numerical fitting parameters[24,50] are employed to fit the measured conductance curves and thus determine the bulk current spin polarization of the sample: the effective temperature T_{eff}; the barrier strength Z, which accounts for the cleanness of the interface (e.g., an infinite Z accounts for a tunnel transport regime); the superconducting gap Δ ($\sim$1.5 meV for elemental bulk niobium); and the spin polarization $P_{\text{ballistic}}$. The dependences of the fitting parameters on the point-contact resistance (R) are plotted in Fig. 11, among with the resulting fits of the raw data, for comparison.

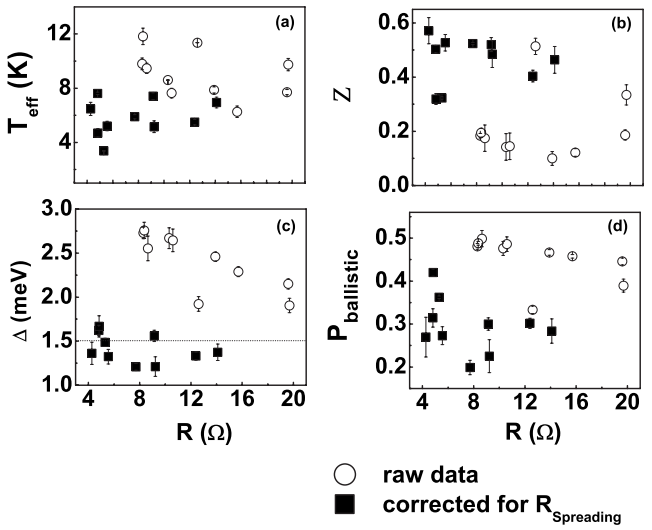

FIG. 11. Dependence of the fitting parameters employed in the modified BTK model, and described in the text, on the point-contact resistance.

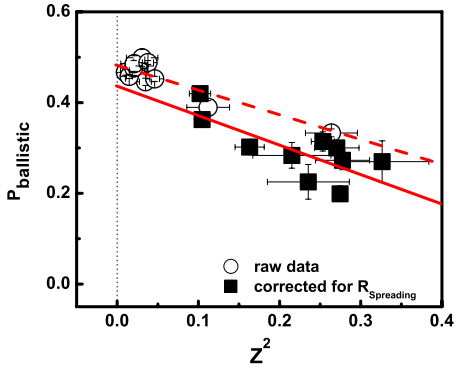

FIG. 12. (Color online) Ballistic current spin polarization vs square of the superconductor-ferromagnet interface transparency parameter Z for $L1_0$-ordered FePt. The extrapolation of the least-squares fit (lines) onto the ordinate gives the bulk spin polarization of the current.

From the data shown in Fig. 11(a), it can be seen that on average T_{eff} is larger than the 4.2 K real temperature of the experiment.[24,52] Such differences between effective and real temperatures have already been reported and are beyond the scope of this paper. They are ascribed to weaknesses in the model since T_{eff} not only accounts for thermal activation but also includes other effects that result in a broadening of the Fermi-Dirac function, such as the electron Fermi velocity mismatch between the tip and the sample, or the presence of a thin remaining oxide layer at the surface. Moreover, this can also represent any spread in the properties of different parallel nanocontacts formed by the tip and sample. To avoid confusion, T_{eff} is sometimes referred to, in the literature, as a broadening factor.

From the data shown in Fig. 11(b), it can be seen that, for a given tip, there is no clear correlation between the point-contact resistance and Z. It had been ascribed to the fact that, for contacts of the same nature, R is mainly determined by the size of the contact rather than its cleanness.[24] As observed in Fig. 11(c), the values of the tip superconducting gaps are in agreement with those of the bulk Nb. Note that the initial large values of the superconducting gap as deduced from fits of the raw data are indeed the signature of spreading resistances. Figure 11(d) shows that the spin polarization does not depend on R in an easily observable way. Rather, note that the fitted spin polarization seems to systematically depend on Z. Here we find an acceptable agreement with a quadratic reduction in $P_{\text{ballistic}}$ with Z,[24,47] as shown in Fig. 12. The relevant value of the spin polarization is known to be the one extrapolated in the case of a perfectly transparent interface (i.e., when $Z=0$). We find a ballistic spin polarization of $P_{\text{ballistic}}=0.42\pm0.05$ for our FePt film.

We note that we obtain similar values of the polarization when we do not apply any correction for the spreading resistance in our FePt film.[49] This value is, moreover, close to that reported for elemental iron using the same technique, i.e., $P_{\text{ballistic}}=0.46\pm0.03$.[52] We have measured a very similar value for a pure Fe film ourselves using the very same experimental setup as in this study, and also shown that it yields a polarization of zero for nonmagnetic materials such as Au. We also note that we obtained the same value, to well within the error bar, when analyzing data taken on the sample in the remanent state or in the ac demagnetized state (PCAR data not shown). As our contact areas are ~10 nm and the domains are ~170 nm across, the likelihood of any given contact touching a wall in the demagnetized film is rather low. Hence most of the data points we used to perform our extrapolation are made in uniformly magnetized regions in both cases, and we would not expect any significant difference arising by this means. Moreover, this method is sensitive only to the magnitude and not the direction of the spin polarization. What is important to notice is that this comparison shows that the effect of any stray fields due to the domain structure on the superconductivity of the tip is negligible.

IV. DISCUSSION AND CONCLUSION

We have determined both the diffusive and ballistic transport spin polarization in high-quality epitaxial sputtered $L1_0$ FePt thin films. In the diffusive electron transport regime, we used magnetoresistance of domain walls along with a modified form of the Levy-Zhang model to determine the spin current asymmetry and hence the diffusive spin polarization of a dc current flowing in $L1_0$ FePt. In the ballistic electron transport regime, we extracted the spin polarization directly from point-contact Andreev-reflection measurements at 4.2 K.

Comparing the polarization in the ballistic transport regime to that in the diffusive, we find that at liquid He temperatures, where the comparison is direct, $P_{\text{diffusive}}$ is substantially higher. In fact, to change the value of $P_{\text{diffusive}}$ to be equal to that measured for $P_{\text{ballistic}}$ by PCAR, it is necessary to change α by a factor of a little over 24. This is because the diffusive polarization is extremely insensitive to α when it is large. While the exact value can be modified by making a different choice for the value of k_F or m, it is not possible to

get a value of $P_{\text{diffusive}}$ that is close to $P_{\text{ballistic}}$ with a physically reasonable set of parameters. To do so, it is necessary to choose a value for m that is less than the free electron mass, extremely unrealistic for a transition metal alloy. With regard to k_F, we chose 2 Å^{-1} as a representative value of k_F for a metal. In order to match the PCAR value of about 40%, we would need k_F=6.9 Å^{-1}, corresponding to an electron density of about 10^{31} m^{-3}, three orders of magnitude too high for a metal, and placing the Fermi surface in the fourth Brillouin zone.

One would not expect that $P_{\text{diffusive}}$ and $P_{\text{ballistic}}$ should be the same in any case. It was pointed out by Mazin[53] that, for a fairly transparent ballistic contact, the conductivity for given spin subband is proportional to $g(E_F)v_F$, whilst for ordinary diffusive transport the conductivity is proportional to $g(E_F)v_F^2\tau$. It is on these parameters that the spin polarization depends:[53] compare Eq. (6) with Eq. (7). The ballistic current polarization is given by

$$P_{\text{ballistic}} = \frac{g_\uparrow(E_F)v_{F,\uparrow} - g_\downarrow(E_F)v_{F,\downarrow}}{g_\uparrow(E_F)v_{F,\uparrow} + g_\downarrow(E_F)v_{F,\downarrow}}. \tag{6}$$

On the other hand, taking into account spin-dependent electron scattering events within the Drude theory, the diffusive current polarization is given by

$$P_{\text{diffusive}} = \frac{g_\uparrow(E_F)v_{F,\uparrow}^2\tau_\uparrow - g_\downarrow(E_F)v_{F,\downarrow}^2\tau_\downarrow}{g_\uparrow(E_F)v_{F,\uparrow}^2\tau_\uparrow + g_\downarrow(E_F)v_{F,\downarrow}^2\tau_\downarrow}, \tag{7}$$

which involves a spin-dependent relaxation time τ, besides the band structure parameters like the density of states $g(E_F)$ and the square of the Fermi velocity v_F. Our work could act as a stimulus for detailed band structure calculations needed to average v_F and v_F^2 over the whole Fermi surface in order to make quantitative comparisons, but we would like to note that the scattering rate $1/\tau$ is seen to be the decisive parameter here. It is not unreasonable to expect that $\tau_\uparrow \neq \tau_\downarrow$ in a ferromagnet such as this, where scattering from defects and impurities occurs at different rates for carriers of different spin.[54] Our parameters for scattering within the FePt metal are within the range of those reported for various impurities introduced as scattering centers into a 3*d* magnetic matrix.[55–57] Moreover, the parameter β that appears in drift-diffusion models of the giant magnetoresistance with the current perpendicular to the plane plays the role of the spin polarization of the diffusive conductivity within the bulk of a magnetic layer. Values for β of up to 0.9 have been found for some commonplace 3*d* ferromagnetic alloys.[58] We therefore explain the much higher values of $P_{\text{diffusive}}$ as compared to $P_{\text{ballistic}}$ as arising from the asymmetry in the scattering rates for spin-up and spin-down carriers from vacancies, impurities, antisite defects in the $L1_0$ structure, and dislocations (as mentioned in the discussion of the HRTEM characterization of our film), which lead to additional polarization in the diffusive current over and above that from the carrier density alone. Meanwhile, only the electronic structure affects the polarization obtained from the PCAR method. It is worth noting that even an unpolarized electron gas can carry a diffusive current of finite spin polarization in the presence of spin-dependent relaxation times. Hence an appropriate ratio of spin-dependent scattering rates can considerably amplify (or, in unfavorable circumstances, attenuate) an intrinsic spin polarization in terms of number density when a current starts to flow.

This is significant, since it is $P_{\text{diffusive}}$ that is the relevant parameter entering into theories of current-driven wall motion;[59–66] indeed it was in this context that Berger suggested, almost 30 years ago, that a measurement of the pressure exerted on a wall in ferromagnet could be used to determine current polarization.[14] We expect that the results of this measurement of $P_{\text{diffusive}}$ should be in accord with that measured by domain wall resistance. However, due to the dearth of experimental data for diffusive values, when experimental data are interpreted in terms of these theories, the lower value of polarization determined from a nondiffusive transport regime such as PCAR is often the only available one to use.[67–70] However, we can see from the results in this paper that these values significantly underestimate the real degree of spin polarization, and hence the rate at which spin angular momentum is transferred to a domain wall. We also anticipate that the diffusive current polarization in more technologically relevant materials such as Permalloy might be measured by making suitable nanostructures that exploit geometrical confinement to form narrow domain walls[71] in order to yield a sufficiently large domain wall resistance to be easily measured.

ACKNOWLEDGMENTS

The authors would like to thank A. T. Hindmarch, G. Burnell, M. Ali, and M. C. Hickey for fruitful discussions. The technical assistance of J. Turton, M. Patel, L. Harris, A. Price, and B. Miller is also gratefully acknowledged. This work was supported by the U.K. EPSRC through the Spin@RT research program. V.B. acknowledges the financial support provided through the European Community's Marie Curie actions (Research Training Networks) under Contract No. MRTN-CT-2003-504462, ULTRASMOOTH.

*phyks@leeds.ac.uk. URL: www.stoner.leeds.ac.uk
†c.h.marrows@leeds.ac.uk

[1] S. Mangin, D. Ravelosona, J. A. Katine, M. J. Carey, B. D. Terris, and E. E. Fullerton, Nat. Mater. **5**, 210 (2006).
[2] P. Caro, A. Cebollada, F. Briones, and M. F. Toney, J. Cryst. Growth **187**, 426 (1998).
[3] T. Suzuki, N. Honda, and K. Ouchi, J. Appl. Phys. **85**, 4301 (1999).
[4] S. Ishio, T. Yoshino, H. Saito, T. Suzuki, and K. Ohuchi, J. Magn. Magn. Mater. **239**, 217 (2002).
[5] M. M. Schwickert, K. A. Hannibal, M. F. Toney, M. Best, L. Folks, J.-U. Thiele, A. J. Kellock, and D. Weller, J. Appl. Phys.

87, 6956 (2000).
[6] K. Barmak, J. Kim, L. H. Lewis, K. R. Coffey, M. F. Toney, A. J. Kellock, and J.-U. Thiele, J. Appl. Phys. **95**, 7501 (2004).
[7] K. Barmak, J. Kim, L. H. Lewis, K. R. Coffey, M. F. Toney, A. J. Kellock, and J.-U. Thiele, J. Appl. Phys. **98**, 033904 (2005).
[8] C. Clavero, J. M. García-Martin, J. L. Costa Krämer, G. Armelles, A. Cebollada, Y. Huttel, R. A. Lukaszew, and A. J. Kellock, Phys. Rev. B **73**, 174405 (2006).
[9] D. Ravelosona, A. Cebollada, F. Briones, C. Diaz-Paniagua, M. A. Hidalgo, and F. Batallan, Phys. Rev. B **59**, 4322 (1999).
[10] J. Yu, U. Rüdiger, A. K. Kent, R. F. C. Farrow, R. F. Marks, D. Weller, L. Folks, and S. S. P. Parkin, J. Appl. Phys. **87**, 6854 (2000).
[11] C. H. Marrows and B. C. Dalton, Phys. Rev. Lett. **92**, 097206 (2004).
[12] C. W. Heaps, Phys. Rev. **45**, 320 (1934).
[13] G. R. Taylor, A. Isin, and R. V. Coleman, Phys. Rev. **165**, 621 (1968).
[14] L. Berger, J. Appl. Phys. **49**, 2156 (1978).
[15] A. D. Kent, J. Yu, U. Rüdiger, and S. S. P. Parkin, J. Phys.: Condens. Matter **13**, 461 (2001).
[16] C. H. Marrows, Adv. Phys. **54**, 585 (2005).
[17] H. Tanigawa, A. Yamaguchi, S. Kasai, T. Ono, T. Seki, T. Shima, and K. Takanashi, J. Appl. Phys. **99**, 08G520 (2006).
[18] W. L. Lee, F. Q. Zhu, and C.-L. Chien, Appl. Phys. Lett. **88**, 122503 (2006).
[19] M. Viret, D. Vignoles, D. Cole, J. M. D. Coey, W. Allen, D. S. Daniel, and J. F. Gregg, Phys. Rev. B **53**, 8464 (1996).
[20] G. G. Cabrera and L. M. Falicov, Phys. Status Solidi B **61**, 539 (1974).
[21] G. G. Cabrera and L. M. Falicov, Phys. Status Solidi B **62**, 217 (1974).
[22] P. M. Levy and S. Zhang, Phys. Rev. Lett. **79**, 5110 (1997).
[23] R. J. Soulen *et al.*, Science **282**, 85 (1998).
[24] G. J. Strijkers, Y. Ji, F. Y. Yang, C. L. Chien, and J. M. Byers, Phys. Rev. B **63**, 104510 (2001).
[25] B. E. Warren, *X-Ray Diffraction* (Addison-Wesley, Reading, MA, 1969).
[26] *International Tables for X-Ray Crystallography*, edited by C. H. Macgillaury, G. D. Rieck, and K. Lonsdale (Kynoch Press, Birmingham, England, 1962), Vol. III.
[27] *International Tables for X-Ray Crystallography*, edited by J. A. Ibers and W. C. Hamilton (Kynoch Press, Birmingham, England, 1974), Vol. IV.
[28] M. MacKenzie, J. N. Chapman, S. Cardoso, H. Li, R. Ferreira, and P. P. Freitas, J. Phys. D **38**, 1869 (2005).
[29] S. Chikazumi, *Physics of Ferromagnetism* (Oxford University Press, Oxford, 1998).
[30] R. F. C. Farrow, D. Weller, R. F. Marks, M. F. Toney, A. Cebollada, and G. R. Harp, J. Appl. Phys. **79**, 5967 (1996).
[31] G. H. O. Daalderop, P. J. Kelly, and M. F. H. Schuurmans, Phys. Rev. B **44**, 12054 (1991).
[32] K. Inoue, H. Shima, A. Fujita, K. Oikawa, K. Fukamichi, and K. Ishida, Appl. Phys. Lett. **88**, 102503 (2006).
[33] S. Okamoto, N. Kikuchi, O. Kitakami, T. Miyazaki, Y. Shimada, and K. Fukamichi, Phys. Rev. B **66**, 024413 (2002).
[34] J.-U. Thiele, L. Folks, M. F. Toney, and D. K. Weller, J. Appl. Phys. **84**, 5686 (1998).
[35] V. Gehanno, A. Marty, B. Gilles, and Y. Samson, Phys. Rev. B **55**, 12552 (1997).
[36] M. Donahue and D. G. Porter, National Institute of Standards and Technology, Interagency Report No. NISTIR 6376, 1999 (unpublished).
[37] B. Kaplan and G. A. Gehring, J. Magn. Magn. Mater. **128**, 111 (1993).
[38] L. Klein, Y. Kats, A. F. Marshall, J. W. Reiner, T. H. Geballe, M. R. Beasley, and A. Kapitulnik, Phys. Rev. Lett. **84**, 6090 (2000).
[39] B. Raquet, M. Viret, P. Warin, E. Sondergard, and R. Mamy, Physica B **294-295**, 102 (2001).
[40] B. Raquet, M. Viret, E. Søndergård, O. Cespedes, and R. Mamy, Phys. Rev. B **66**, 024433 (2002).
[41] M. W. Stringfellow, J. Phys. C **1**, 950 (1968).
[42] A. B. Pippard, *Magnetoresistance in Metals*, Cambridge Studies in Low Temperature Physics (Cambridge University Press, Cambridge, UK, 1989).
[43] J. M. MacLaren, R. R. Duplessis, R. A. Stern, and S. Willoughby, IEEE Trans. Magn. **41**, 4374 (2005).
[44] M. J. M. de Jong and C. W. J. Beenakker, Phys. Rev. Lett. **74**, 1657 (1995).
[45] S. K. Upadhyay, A. Palanisami, R. N. Louie, and R. A. Buhrman, Phys. Rev. Lett. **81**, 3247 (1998).
[46] B. Nadgorny, I. I. Mazin, M. Osofsky, R. J. Soulen, P. Broussard, R. M. Stroud, D. J. Singh, V. G. Harris, A. Arsenov, and Y. Mukovskii, Phys. Rev. B **63**, 184433 (2001).
[47] Y. Ji, G. J. Strijkers, F. Y. Yang, C. L. Chien, J. M. Byers, A. Anguelouch, G. Xiao, and A. Gupta, Phys. Rev. Lett. **86**, 5585 (2001).
[48] A. F. Andreev, Sov. Phys. JETP **37**, 5015 (1988).
[49] G. T. Woods, R. J. Soulen, Jr., I. I. Mazin, B. Nadgorny, M. S. Osofsky, J. Sanders, H. Srikanth, W. F. Egelhoff, and R. Datla, Phys. Rev. B **70**, 054416 (2004).
[50] Y. Bugoslavsky, Y. Miyoshi, S. K. Clowes, W. R. Branford, M. Lake, I. Brown, A. D. Caplin, and L. F. Cohen, Phys. Rev. B **71**, 104523 (2005).
[51] G. E. Blonder, M. Tinkham, and T. M. Klapwijk, Phys. Rev. B **25**, 4515 (1982).
[52] C. H. Kant, O. Kurnosikov, A. T. Filip, P. LeClair, H. J. M. Swagten, and W. J. M. de Jonge, Phys. Rev. B **66**, 212403 (2002).
[53] I. I. Mazin, Phys. Rev. Lett. **83**, 1427 (1999).
[54] R. C. O'Handley, *Modern Magnetic Materials: Principles and Applications* (Wiley, New York, 2000).
[55] I. A. Campbell and A. Fert, *Ferromagnetic Materials* (North-Holland, Amsterdam, 1982), Vol. 3, p. 747.
[56] H. A. M. van den Berg, *Magnetic Multilayers and Giant Magnetoresistance: Fundamentals and Industrial Applications*, Springer Series in Surface Sciences Vol. 37 (Springer-Verlag, Berlin, 2000), p. 215.
[57] J. W. F. Dorleijn, Philips Res. Rep. **31**, 287 (1976).
[58] J. Bass and W. P. Pratt, J. Magn. Magn. Mater. **200**, 274 (1999).
[59] G. Tatara and H. Kohno, Phys. Rev. Lett. **92**, 086601 (2004).
[60] S. Zhang and Z. Li, Phys. Rev. Lett. **93**, 127204 (2004).
[61] Z. Li and S. Zhang, Phys. Rev. Lett. **92**, 207203 (2004).
[62] A. Thiaville, Y. Nakatani, J. Miltat, and N. Vernier, J. Appl. Phys. **95**, 7049 (2004).
[63] A. Thiaville, Y. Nakatani, J. Miltat, and Y. Suzuki, Europhys. Lett. **69**, 990 (2005).
[64] Y. Tserkovnyak, H. J. Skadsem, A. Brataas, and G. E. W. Bauer, Phys. Rev. B **74**, 144405 (2006).
[65] A. Vanhaverbeke and M. Viret, Phys. Rev. B **75**, 024411 (2007).

[66] B. Krüger, D. Pfannkuche, M. Bolte, G. Meier, and U. Merkt, Phys. Rev. B **75**, 054421 (2007).
[67] G. S. D. Beach, C. Knutson, C. Nistor, M. Tsoi, and J. L. Erskine, Phys. Rev. Lett. **97**, 057203 (2006).
[68] L. Thomas, M. Hayashi, X. Jiang, R. Moriya, C. Rettner, and S. S. P. Parkin, Nature (London) **443**, 197 (2006).
[69] M. Hayashi, L. Thomas, C. Rettner, R. Moriya, Y. B. Bazaliy, and S. S. P. Parkin, Phys. Rev. Lett. **98**, 037204 (2007).
[70] G. Meier, M. Bolte, R. Eiselt, B. Krüger, D. H. Kim, and P. Fischer, Phys. Rev. Lett. **98**, 187202 (2007).
[71] P. Bruno, Phys. Rev. Lett. **83**, 2425 (1999).